Is it possible to unambiguously assess the presence of two defects by temperature and injection dependent lifetime spectroscopy?

Tine. U. Nærland, Simone Bernardini, Marie Syre Wiig, and Mariana I. Bertoni

***Abstract*—The work presented herein comprehends a systematic study of the prospects for an unambiguous assessment of the presence of two separate defects in silicon samples analyzed by temperature and injection dependent lifetime spectroscopy. A large number of lifetime data sets are generated by simulating the presence of two defects and then fitted to a single defect lifetime model. We have categorized the outcome in four categories: (i) a low overall fit quality and thus likely a combination of two defects, (ii) a high overall fit quality by dominance of one of the involved defect, (iii) a high overall fit quality because of symmetry effects in the model, and (iv) a high overall fit quality but no clear dominance by either involved defects nor presence of symmetry effects. We show that the presence of two defects can be ascertained through perceiving a low-quality fit to a single defect model (category (i)), but we also show that a high-quality fit can arise from a combination of two defects (category (iv)). We show that in the case of category (i) and (iv) it is possible to identify the two original defects through linear parametrization. In the case of (iii), however, the identification of two simultaneously occurring defects is highly ambitious and not practically feasible.**

***Index Terms*—Bulk lifetime, defects in silicon, defect parameter contour mapping (DPCM), lifetime spectroscopy, simulation, Shockley-Read-Hall (SRH)theory – modeling, temperature- and injection-dependent lifetime spectroscopy (TIDLS)**

I. Introduction

During the last 25 years, there has been a vast number of reports using Shockley-Read-Hall (SRH) theory [1], [2] to determine defect parameters in silicon from minority carrier lifetime measurements. In some of these studies, the contaminant/defect is intentionally introduced in large amounts so that it can be assumed that the introduced contaminant is indeed representing the lifetime dominating defect [3]-[14]. In other cases the contaminant is unknown [15]-[21], and in some cases the authors assume the presence of more than one lifetime reducing defect and consequently fit the lifetime curves with a combination of defects [3]-[9], [13], [15], [22], [23]. The questions we pose herein are: How ambiguous, or not, is this kind of fitting? What are the potential pitfalls? In this contribution, we are using our recently introduced defect parameter contour mapping (DPCM) method [18], [24], [19] to assess these questions using simulated lifetime data.

II. Defect parameter contour mapping

Defect parameter contour mapping (DPCM) is based on using SRH theory to calculate the fit quality of a simulated curve to a measured curve, for a given range of values for the defect energy level (E_t) and the capture cross-section ratio (k). For every $E_t - k$ combination the time constants τ_{p0} and τ_{n0} are varied until the best fit of the experimental data is obtained. The quality of the fit is determined by calculating an *Average Residual Value (ARV):*

$$\boldsymbol{Average\ Residual\ Value} = \sum_{j=1}^{m}\left(\left(\sum_{i=1}^{n}\frac{\left|\tau_{measured,j}-\tau_{model,j}\right|}{\tau_{measured,j}}\right)/n\right)/m \quad (1)$$

where n is the number of injection level values and m is the number of temperatures taken into account. Advantages of using DPCM (and other lifetime spectroscopy methods that utilize E_t and k parametrization) to determine electronic properties of defects are that no prior knowledge of the defect concentration is required and that we do not simplify the SRH-

This project is funded by the Engineering Research Center Program of the National Science Foundation and the Office of Energy Efficiency and Renewable Energy of the Department of Energy under NSF Cooperative Agreement No. EEC-1041895. Any opinions, findings and conclusions or recommendations expressed in this material are those of the author(s) and do not necessarily reflect those of the National Science Foundation. Part of this work was performed within the Norwegian Research Centre for Sustainable Solar Cell Technology (FME SuSolTech, project number 257639), co-sponsored by the Norwegian Research Council and research and industry partners.

Tine U. Nærland, Simone Bernardini, and Mariana I. Bertoni are with Ira A. Fulton Schools of Engineering, Arizona State University, Tempe, AZ 85287, USA. (E-mail: tine.uberg@gmail.com; simone.bernardini@asu.edu; bertoni@asu.edu). Marie Syre Wiig is with the Department of Solar Energy, Institute for Energy Technology, Instituttveien 18, 2007 Kjeller, Norway. (E-mail: marie.syre.wiig@ife.no)

equation for high or low injection range conditions with the uncertainty that this introduces. Compared to the Defect Parameter Solution Surface (DPSS) method [25] DPCM has the advantage that the extent and measure of the local minima of the fitting procedure are given directly in the plot by the brightness without introducing additional complementary plots. The DPCM code provides the magnitude of the min ARV and the corresponding E_t and k values for as many bright regions as the user desires, just as in the recently introduced Newton-Raphson method [26]. The computing time for the plots can be adjusted (from seconds to an hour) depending on the desired resolution and range. More detailed descriptions on the DPCM-method can be found in Ref. [18] and [24].

III. Approach

To investigate how the lifetime curves are affected by the presence of two simultaneously occurring defects we have simulated 36 combinations of 9 different defects in p-type silicon ($N_a = 2 \times 10^{15}$ cm^{-3}). To assert a good representation of the defect energy levels (E_t) and capture cross-section ratios (k) we have chosen a set of defects that serves to exemplify the diversity in E_t and k space. The defects of choice are listed in *Table 1* with their respective E_t and k-values. No suitable defect was found to represent a mid-band gap defect with a k-value of approximate unity. Hence, a defect denoted as "DefectX" was created to represent this E_t and k combination.

Table 1 The nine different defects used to simulate two-defect lifetime limited data. Their individual E_t and k-values are as found in literature and can be displayed in E_t and k-space as in the plots in Fig. 1. The defect concentration, N_t, listed, is for the respective pure defects alone (100%), based on a lifetime of 50 µs at 5×10^{14} cm^{-3} at 25°C as shown in Fig. 1.

Impurity	E_t ($E_{defect} - E_V$) [eV]	$k = \sigma_n/\sigma_p$	σ_p [cm^2]	N_t	Ref
Cu(I)	0.92	0.05	3×10^{-17}	6×10^{13}	[5]
Cu(II)	0.62	16.0	1×10^{-19}	2×10^{16}	[5]
Pt(I)	0.32	0.01	8.4×10^{-15}	2×10^{11}	[27]
Ti	0.85	22.0	1.4×10^{-15}	1×10^{12}	[29]
Mo	0.28	30.0	6×10^{-16}	3×10^{13}	[29]
Zn	0.33	0.34	4.4×10^{-15}	4×10^{11}	[29]
Pt(II)	0.89	1.12	2.6×10^{-14}	7×10^{10}	[27]
Au	0.57	0.02	7.6×10^{-15}	2×10^{11}	[27]
DefectX	0.56	1.0			

The simulation of lifetime curves was achieved by using SRH theory [1], [2] to model the effective lifetime vs. injection level curves at different temperatures according to:

$$\frac{1}{\tau_{eff}} = \frac{1}{\tau_{SRH,1}} + \frac{1}{\tau_{SRH,2}} \quad (2)$$

where

$$\tau_{SRH} = \frac{\tau_{n0}(N_A + p_1 + \Delta n) + \tau_{p0}(n_1 + \Delta n)}{N_A + n_0 + \Delta n} \quad (3)$$

For every combination of two of the defects in Table 1, we simulated the lifetime vs. injection level curves at seven different temperatures ranging from 25 – 230˚C, which is the temperature range of our Sinton WCT-120TS lifetime tester setup. Using the relation $\tau_{p0} = 1/N_t\sigma_p v_{th}$ we simulated the lifetime curves corresponding to different ratios of the $N_t\sigma_p$ -product for the two defects. We chose nine points evenly spaced across the tie line defined by the linear combination of both defects (from 0 – 100% of one of the defects). This was done by tuning the ratio between the τ_{p0}'s of the two combined defects, since τ_{p0} is proportional to N_t when σ_p and v_{th} are kept fixed. Furthermore, to assure that all the lifetime curve sets would fall in the τ_{p0} range covered by our "universal case" DPCM analysis we chose τ_{p0} values that would give us a lifetime curve at room temperature equaling approximately 50 µs at 5×10^{14} cm^{-3} (the mid-point of the injection range for the DPCM analysis). The corresponding concentrations of the defects are given in Table 1. Note that for this kind of examination it is the net influence on the lifetime curve (the product of $N_t\sigma_p$) that is interesting, not N_t itself.

In total, we generated 36 combinations of different defects, each in 9 ratios, adding up to 261 unique temperature-dependent lifetime curve-sets. For each of the lifetime curve-sets, we then generated a contour plot and determined the E_t and k-value giving the best fit to a one defect lifetime-model. In this analysis, where we look at synthetic SRH lifetime data, we are not taking into account surface, Auger, and radiative recombination. When analyzing experimental data, however, these mechanisms need to be included in the DPCM analysis, like in [18], [19] and [22].

All the simulated curve sets, DPCM plots, and code are available through [28]. The lifetime curve sets and DPCM plots for the nine single defects (free of the impact of a second defect) are given in Fig. 1.

IV. Results and Discussion

In the following, we will look at the min ARV, the E_t, and the k-value obtained from analyzing lifetime data given by the convolution of two defects when applying a one-defect model. First of all, we discuss the importance of the symmetry areas that can be observed in the DPCM plots. Then we will look into whether the quality of the fit alone, namely the min ARV, can indicate the occurrence of multiple defects. Lastly, we will investigate linear parametrization and the possibility of comparing the analyses of restricted regimes of the injection level, as a method to identify the presence of multiple defects.

A. *The Symmetry Effect*

Studying the plots in Fig. 1 made from the single defects in Table 1, they all have bright regions corresponding to the E_t and k parameters of the defect used to simulate the data (circled in red). The overlap between the bright region and the annotated defect location verifies the validity of the method. However, for

most of the plots, it can also be observed that there are other bright regions - not corresponding to the defect parameters of the defect that was simulated – indicating erroneous fits. An example of this can be observed in Fig. 1 a): As expected the plot generates a region of a good fit at the correct E_t and k-values of Cu(I), but other regions of seemingly good fits can also be observed: There is one bright region corresponding to a low defect energy and a high k-value in the lower right corner, and also one bright region with the same k-value as the "correct" parameter set, but with E_t levels in the opposite bandgap half.

What we observe are symmetry effects in the parameter space: Certain combinations of E_t and k parameters produce almost the exact same lifetime data, giving rise to multiple bright regions in the DPCM plot, e.g., the DPCM plots and lifetime curves for Fig. 1 a) g) and h). This is due to the SRH-equation itself and the physical nature of the band gap. A detailed analysis on these matters can be found in Rein's book [30].

This, in turn, means that some of the most common defects could generate very similar contour plots and thus there is no physical way by lifetime spectroscopy alone to know whether only one or more defects are occurring. An example of this is given in Fig. 2 where the combination of Cu(I) and Pt(I) from Table 1 is analyzed. Fig. 2 a) shows the simulated raw data for the combination of defects (again, these are very similar to the lifetime plots in 1 a), g) and h). Further on, the DPCM plot (Fig. 2 c)) is shown, illustrating the high quality of the fit by the white color. In b) linearization as in Ref. [23] is shown. The linearity of the curves indicates the presence of a single defect. In Fig. 2 d) a DPSS and a standard deviation plot as in Ref. [25] is similarly indicating a good fit and no ambiguity. The symmetry effect results in situations where multiple defects appear as one defect.

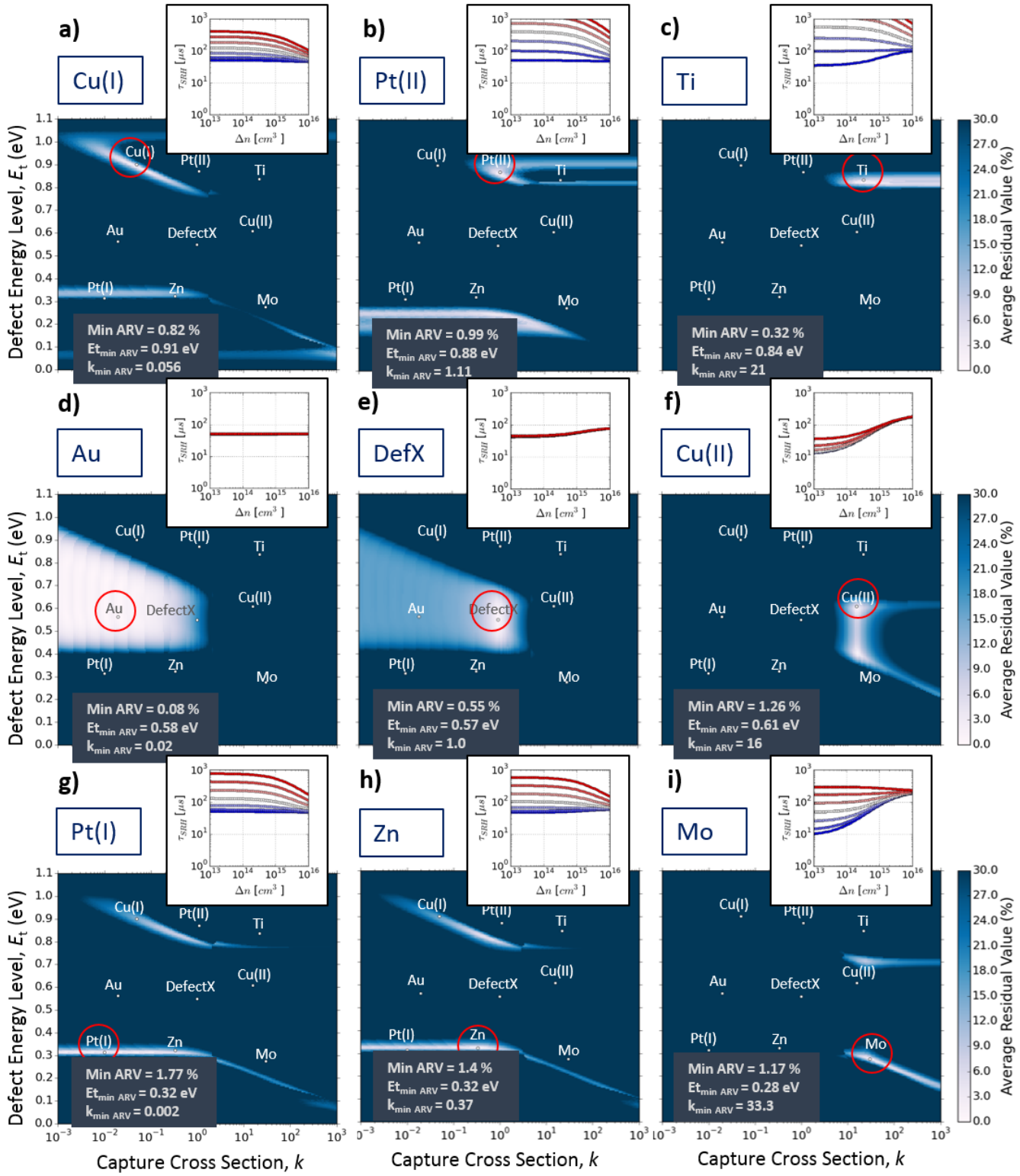

Fig. 1 DPCM and corresponding lifetime plots for the nine single defects listed in *Table 1*. The defect being simulated and analyzed is circled in red. Bright regions indicate E_t and k combinations giving the best fit.

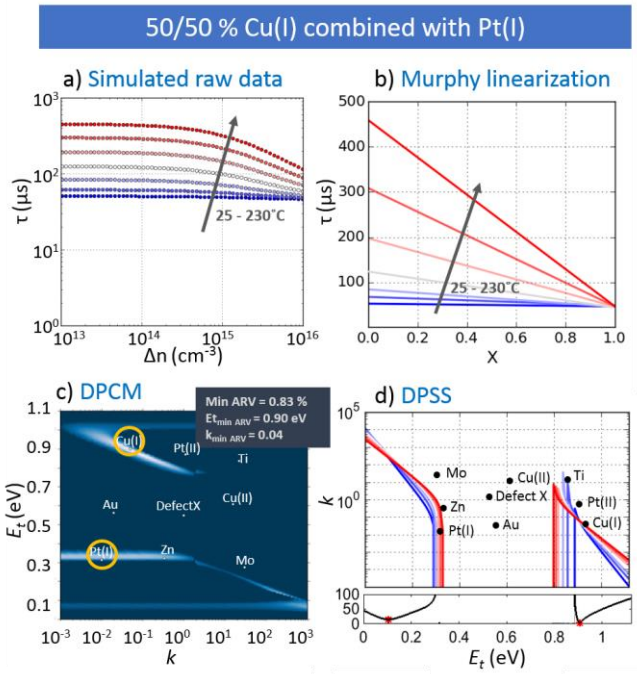

Fig. 2 (a) Simulated lifetime curves for a 50/50% combination of Cu(I) and Pt(I). (b) Murphy linearization of the lifetime curves in a), is showing no evidence of two defects occurring. c) and d) are corresponding DPCM and DPSS analysis for the curve set in a), both indicating good one-defect fit quality. The color scale for the DPCM plot is the same as in Fig 1. In Fig 2 d) the lower sub plot shows the relative standard deviation in the DPSS curves.

In the further assessment of backtracking the two defects in the combinations made, we are disregarding the combinations of defects that fall on the symmetry lines/areas of each other, (e.g. Cu(I) and Pt(I), Cu(I) and Zn, and, Zn and Pt(I)), as these combinations occur as single defects.

B. Investigation of the minimum ARV as an indicator of one or multiple defects

In the DPCM plots, the quality of the fit is represented by calculating an ARV which is a measure of the mismatch of the "measured" (in this case simulated) and a modeled curve. Since the DPCM method is based on fitting lifetime curves, at different temperatures, with a one defect model, it is anticipated that lifetime curves associated to a single defect would result in an overall better fit than lifetime curves associated to more than one defect. The hypothesis is thus that: **If there is a combination of defects, we would expect the min ARV to be larger than for a single defect when fitting to a one defect model.**

To test this hypothesis, we investigated the minimum ARV for 261 unique DPCM plots produced as described in section *III*. The results were categorized into the following categories:

(i) *high min ARV* (low-quality fit and thus likely a combination of two defects),

(ii) *dominated* (low min ARV but positioned close to either of the "mother defects" involved in the combination),

(iii) *symmetry* (low min ARV but symmetry regions overlapping with either of the mother defects) and,

(iv) *low min ARV* (but no occurrence of dominance or symmetry effects).

The conditions for category (iii) were covered in *IV A*. In this section, we will discuss category (ii): Dominance by one of the defects.

When combining defects, there will often be one defect that is so much more recombination active than the other that it becomes the only defect detectable by LS methods. Notice that, in this case, the LS plot still produces a meaningful result in terms of pointing us to the parameters of the lifetime dominating defect. An example is given in Fig. 3 where combinations of different fractions of the defects Pt(I) and DefectX are shown, all of them with a best fit coinciding to DefectX, even at 87.5% Pt(I). This is typical for category (ii) defects.

In the case of p-type silicon, the dominating defects are typically, but not exclusively, the ones with the higher *k*. (The

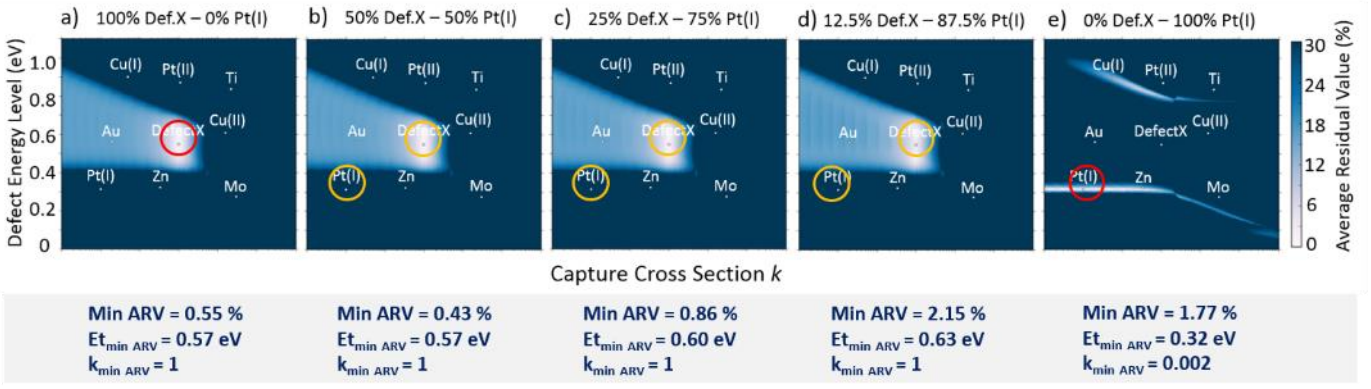

Fig. 3 a) – e) shows the transition from 100% DefectX to 100% Pt(I). The sequence of pictures shows that DefectX is completely dominating at all fractions due to DefectX's higher *k*-value and "deeper" E_t - value. Red circle indicates that the defect is the sole defect in play. Yellow circle indicates that there are multiple defects in play. The magnitude of min ARV and the E_t and *k* values at which the min ARV is found are given below each map.

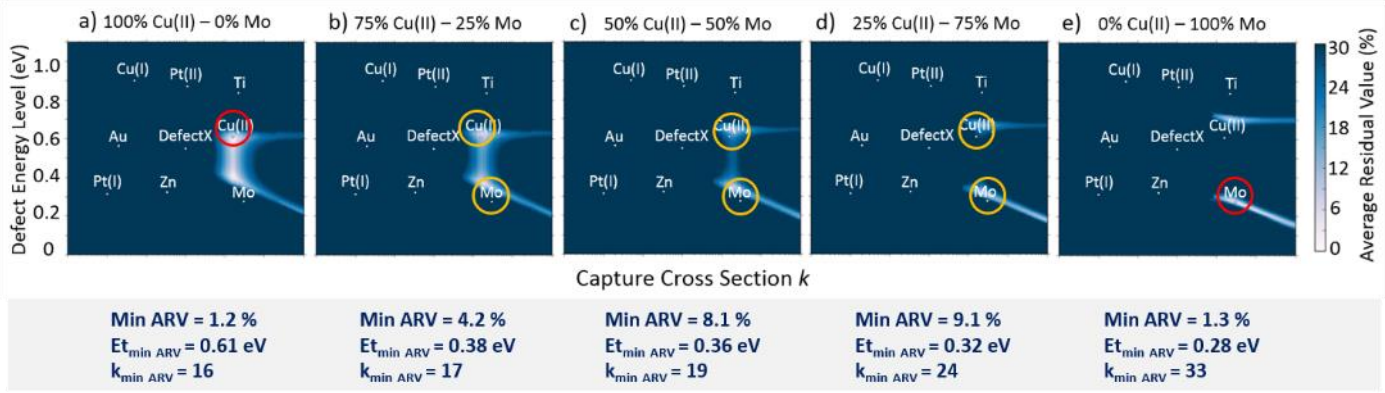

Fig. 4 a) – e) shows the transition from 100% Cu(II) to 100% Mo. The sequence of pictures shows how the bright region of good fit changes location in E_t and k space during the transition. In b) – d) the location of the bright region is neither pointing to the Cu(II)-defect nor the Mo-defect. The magnitude of min ARV and the E_t and k values at which the min ARV is found are given below each map.

opposite would be the case in n-type.) When combining defects with a similar k-value, on the other hand, the transition in the location of the bright region is more gradual, even if one of the defects is located deeper in the band gap and thus represent a more effective recombination site. This kind of gradual change can be observed in the case of combining Cu(II) and Mo in Fig. 4.

In the 252 plots of unique combinations of defects, 122 of the combinations fall into the criterion of shifting less than 25 meV or 0.5 decades k away from either of the two mother defects (cat. (ii)). Another 50 fall into the criterion of not moving out of the symmetry areas/lines of one of the mother defects (cat. (iii)).

For the analysis of the rest of the combinations, we are interested to know if there are combinations of defects producing a bright region with low ARV that does not coincide to either of the mother defects. If such cases exist, this is interesting from the point of view that lifetime spectroscopy analysis in such cases can generate a misconception of a false

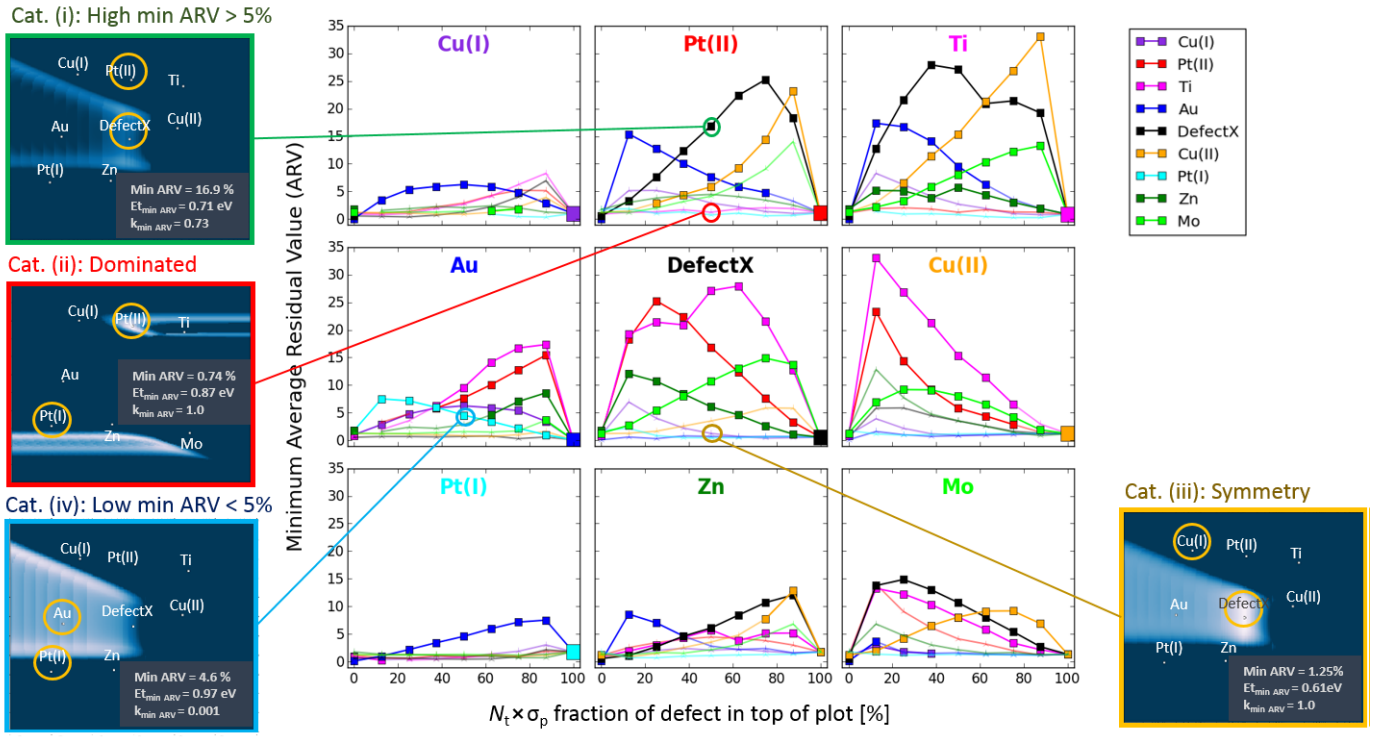

Fig. 5 Sub-plots showing the min ARV as a function of the concentration fraction. 100% concentration fraction represents the defect annotated in the top of the plot. The color of the curves indicate the defect that the annotated defect is combined with. Translucent curves with tripod-markers instead of squares indicates that the combination of defects falls into category (ii) or (iii). The DPCM plots on the sides are examples of the four categories of outcomes.

defect that is merely a random product from analyzing lifetime data influenced by two other defects.

In Fig. 5 we are displaying the min ARV extracted from the 261 generated DPCM plots. The nine sub plots are showing the minimum ARV (y-axis) produced when combining each of the nine defects in Table 1 with the other eight defects at different fractions (x-axis). Note that there are 36 unique elemental combinations. In each plot, the 100% fraction is given by the defect annotated at the top of the plot. The differently colored curves point to the particular defect to which the annotated defect is combined with. In the cases where the E_t and k values from the maps are coinciding with one of the mother defects by either dominance or symmetry effects (category (ii) or (iii)) the points and the line in between them is made translucent. Examples of DPCM maps for each category are displayed in Fig. 5.

From Fig. 5 it is obvious that the combined defects, in general, show a higher ARV (>5%) than the pure defects (at 0 and 100%). There are, however, cases of low ARV, even for combinations of defects, e.g., in the example in the blue frame in the lower left corner of Fig. 5 where the min ARV < 5% despite having 50% of one defect and 50% of another. These cases are, however, rare; in Fig. 6 we have categorized the 50/50% fraction of all the 36 elemental combinations into the categories introduced in *VI B.*

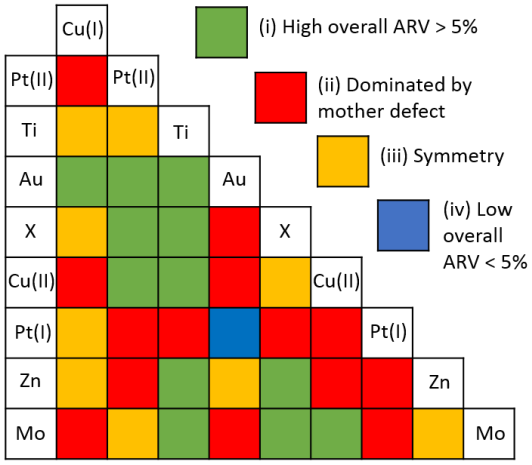

Fig. 6 Classification of the 50/50% fraction for the 36 elemental combinations. More than half of the cases are characterized by that category (ii) that one of the mother defects is dominating the recombination properties of the combination or category (iii) that the characteristics of the fit of the combination curves is coinciding with the symmetry regions of the mother defect and so cannot be identified.

As shown in Fig. 6 there is only one case (i.e. one blue square) where the combination of defects at 50% fraction produces a map with a low min ARV when the bright region cannot be associated with any of the mother defects (category (iv)). From Fig. 1. we can establish that all the pure defects produce a min ARV below 5%. For the synthetic data used in this study, we can conclude that for a DPCM plot with a min ARV above 5% this points towards the presence of multiple defects. When analyzing experimental data, however, there is an experimental uncertainty involved of approx. 10 % [31]. In this case the threshold for pointing out the presence of multiple defects adds up to 5 + 10 = 15%. A low ARV value < 5% (< 15% for experimental data) generally points toward the dominance of one particular defect.
In the next section, we will investigate if there are ways to identify the mother defects in the category (i) and (iv) cases.

C. Identifying simultaneously occurring defects

When two or more defects are present at the same time, the resulting lifetime curves are given by the convolution of the individual defects features. Unless the lifetime curves of the defects involved have the exact same shape (symmetry effects), as discussed in section *IV A.*, the influence of the defect with the E_t - k combination producing the steepest curve (with positive slope) would be stronger in the low injection regime and vice versa in the high injection regime.
For the following investigation, we are looking at two different cases: one case from category (i) *high min ARV*, and the one case from category (iv) *low min ARV* (but not affected by dominance or symmetry effects).

In Fig. 7 a) the case of DefectX mixed with Pt(II) is investigated (the example used for cat. (i) in Fig. 5). In this case, the min ARV of the plot is 16.9% and, following the discussion in section *IV B.*, we obviously would expect the presence of more than one defect. Fig. 7 a II) shows the lifetime parameterized as a function X = n/p according to Murphy [23], and the presence of more than one defect is obvious as the data cannot be fitted to one linear expression. The data can be fitted by a harmonic sum of two linear expressions as shown for a single temperature in the Fig. 7 a II) inset. Using the lifetime data from the linear parametrization when assuming two defects, two individual DPCM-plots can be produced. The resulting plots are shown in Fig. 7 a III and IV) and from the bright regions, we can see that we have obtained an overlap with the mother defects. For comparison, in Fig. 7 a V and VI) we have used the DPCM method to investigate if we, by simply analyzing the lifetime data in high and low injection ranges, can point out the mother defect. The results show that this approach works for neither the low injection regime nor the high injection regime as the bright regions of the plots are far off the mother defects indicated by the yellow circles. The impact of the other defect can hence not be accounted as negligible in either low injection or high injection in this case.
In Fig. 7 b) the case of 50/50% Au combined with Pt(I) is shown. This is the category (iv) example from Fig. 5 where the ARV is below 5% but not related to symmetry effects or dominance. The DPCM plots from the linear parametrization

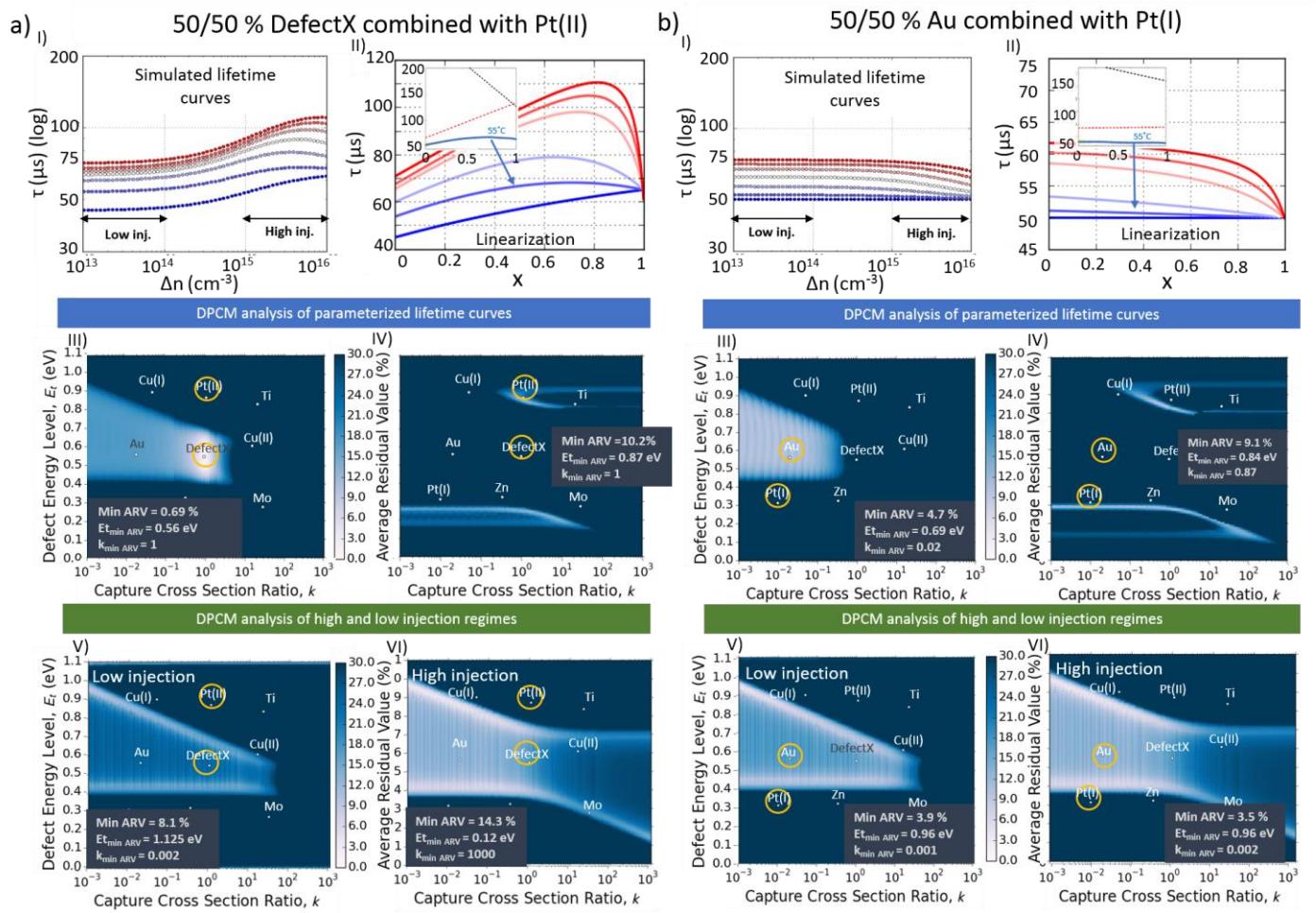

Fig. 7 a) and b). Examples of category (i) and (iv), respectively. In plot I) and II) raw lifetime data and linearization by the Murphy method are shown. The insets are showing the two linear expressions shown for a single temperature. In III) and IV) DPCM analysis from the linearized parametrization (averaging over the parametrized curves for the seven temperatures) assuming two defects, are shown, both able to intersect the involved defects (mother defects) in the lifetime data (yellow circles). In V) and VI) DPCM is used to investigate if simply analyzing the lifetime data in high and low injection regimes can unravel the mother defects, but as the plots are showing, there is no designation to neither of the mother defects (yellow circles) by this approach.

assuming two defects show also here that the mother defects can be tracked as long as enough temperature data is available (the parametrization of the lifetime curves close to room temperature is close to linear). The approach of simply analyzing the lifetime in high and low injection regimes as in Fig. 7 b V and VI) shows again that this approach is not viable. What should be noted here, though, is that this approach will be increasingly valid the bigger difference between the E_t-value of the two involved defects there is. This threshold-value is still under investigation and will be included in a later paper. Nevertheless, what we have shown here is that in the cases where two defects are occurring simultaneously, individually affecting the shape of the lifetime curves, it is possible to backtrack the identity of the two by linearization in combination with a LS method such as DPCM.

V. Conclusion

In this work, we have modeled the temperature dependent minority carrier lifetime of 261 cases of single and combined defects. The lifetime data is analyzed by fitting to a one defect model, where a good quality fit is represented by a low Average Residual Value (ARV).The outcomes were categorized into the following categories: (i) *high min ARV* (low quality fit and thus likely a combination of two defects), (ii) *dominated* (low min ARV but E_t and k parameters close to either of the mother defects), (iii) *symmetry* (low min ARV but symmetry regions overlapping with mother defect.) and (iv) *low min ARV* (but not affected by dominance or symmetry effects).

We show that the presence of two defects can be ascertained by determining a low-quality fit to a single defect model (category (i)), but we also show that a high-quality fit can arise from a combination of defects (category (ii), (iii) and (iv)). For those combinations of defects that do not fall into category (ii) and

(iii) the mother defects can be tracked by linear parametrization as long as sufficient temperature data is available. Another important outcome of this study is the reminder that two contributing defects will appear like one single defect if they have E_t and k-values corresponding to symmetry areas of each other. It is, therefore, good practice in defect identification by TIDLS to map the theoretical areas of symmetry (by, e.g., DPCM), for the suspected defect, to achieve awareness of possible simultaneously occurring defects.

ACKNOWLEDGEMENT

The authors would like to thank Jan-Erik Carlsen for help with the coding.

REFERENCES

[1] R. N. Hall, "Electron-Hole Recombination in Germanium," *Phys. Rev.*, vol. 87, *(2)*, pp. 387-387, 07/1952. DOI: 10.1103/PhysRev.87.387

[2] W. Shockley and W. T. Read, "Statistics of the Recombination of Holes and Electrons," *Phys. Rev.*, vol. 87, *(5)*, pp. 835-842, 09/1952. DOI: 10.1103/PhysRev.87.835

[3] D. Macdonald, A. Cuevas and J. Wong-Leung, "Capture cross sections of the acceptor level of iron–boron pairs in p-type silicon by injection-level dependent lifetime measurements," *J. Appl. Phys.*, vol. 89, *(12)*, pp. 7932-7939, 06/2001. DOI: 10.1063/1.1372156.

[4] J. Schmidt, R. Krain, K. Bothe, G. Pensl and S. Beljakowa, "Recombination activity of interstitial chromium and chromium-boron pairs in silicon," *J. Appl. Phys.*, vol. 102, *(12)*, pp. 123701, 10/2007. DOI: 10.1063/1.2822452

[5] D. Macdonald, W. Brendle, A. Cuevas and A. A. Istratov, "Injection dependent lifetime studies of copper precipitates in silicon," in *12th Workshop Crystalline Silicon Solar Cell Materials and Processes*, Golden, Colorado, pp. 201-204, 2002

[6] S. Diez, S. Rein, T. Roth and S. W. Glunz, "Cobalt related defect levels in silicon analyzed by temperature- and injection-dependent lifetime spectroscopy," *J. Appl. Phys.*, vol. 101, *(3)*, pp. 033710, 02/2007. DOI: 10.1063/1.2433743

[7] S. Dubois, O. Palais and P. J. Ribeyron, "Determination at 300K of the hole capture cross section of chromium-boron pairs in p-type silicon," *Appl. Phys. Lett.*, vol. 89, *(23)*, pp. 232112, 12/2006. DOI: 10.1063/1.2402261

[8] J. Schmidt and D. H. Macdonald, "Recombination activity of iron-gallium and iron-indium pairs in silicon," *J. Appl. Phys.*, vol. 97, *(11)*, pp. 113712, 06/2005. DOI: 10.1063/1.1929096

[9] T. Roth, P. Rosenits, S. Diez, S. W. Glunz, D. Macdonald, S. Beljakowa and G. Pensl, "Electronic properties and dopant pairing behavior of manganese in boron-doped silicon," *J. Appl. Phys.*, vol. 102, *(10)*, pp. 103716, 11/2007. DOI: 10.1063/1.2812698

[10] B. B. Paudyal, K. R. McIntosh and D. H. Macdonald, "Temperature dependent carrier lifetime studies on Ti-doped multicrystalline silicon," *J. Appl. Phys.*, vol. 105, *(12)*, pp. 124510, 06/2009. DOI: 10.1063/1.3139286

[11] B. B. Paudyal, K. R. McIntosh, D. H. Macdonald and G. Coletti, "Temperature dependent carrier lifetime studies of Mo in crystalline silicon," *J. Appl. Phys.*, vol. 107, *(5)*, pp. 054511, 03/2010. DOI: 10.1063/1.3309833

[12] C. Sun, F. E. Rougieux, J. Degoulange, R. Einhaus and D. Macdonald, "Reassessment of the recombination properties of aluminium–oxygen complexes in n- and p-type Czochralski-grown silicon," *Physica Status Solidi (B)*, vol. 253, *(10)*, pp. 2079-2084, 08/2016. DOI: 10.1002/pssb.201600363

[13] J. Schmidt, "Temperature- and injection-dependent lifetime spectroscopy for the characterization of defect centers in semiconductors," *Appl. Phys. Lett.*, vol. 82, *(13)*, pp. 2178-2180, 03/2003. DOI: 10.1063/1.1563830

[14] A. Inglese, J. Lindroos, H. Vahlman and H. Savin, "Recombination activity of light-activated copper defects in p-type silicon studied by injection- and temperature-dependent lifetime spectroscopy," *J. Appl. Phys.*, vol. 120, (12), pp. 125703, 09/2016. DOI: 10.1063/1.4963121

[15] S. Rein and S. W. Glunz, "Electronic properties of the metastable defect in boron-doped Czochralski silicon: Unambiguous determination by advanced lifetime spectroscopy," *Appl. Phys. Lett.*, vol. 82, (7), pp. 1054-1056, 02/2003. DOI: 10.1063/1.1544431

[16] A. E. Morishige, M. A. Jensen, D. B. Needleman, K. Nakayashiki, J. Hofstetter, T. T. A. Li and T. Buonassisi, "Lifetime Spectroscopy Investigation of Light-Induced Degradation in p-type Multicrystalline Silicon PERC," IEEE Journal of Photovoltaics, vol. 6, (6), pp. 1466-1472, 09/2016. DOI: 10.1109/JPHOTOV.2016.2606699

[17] M. A. Jensen, A. E. Morishige, J. Hofstetter, D. B. Needleman and T. Buonassisi, "Evolution of LeTID Defects in p-Type Multicrystalline Silicon During Degradation and

Regeneration," *IEEE Journal of Photovoltaics,* vol. PP, *(99),* pp. 1-8, 03/2017. DOI: 10.1109/JPHOTOV.2017.2695496

[18] S. Bernardini, T. U. Nærland, A. L. Blum, G. Coletti and M. I. Bertoni, "Unraveling bulk defects in high-quality c-Si material via TIDLS," *Prog Photovoltaics Res Appl,* vol. 25, *(3),* pp. 209-217, 12/2016. DOI: 10.1002/pip.2847

[19] T. U. Nærland, S. Bernardini, H. Haug, S. Grini, L. Vines, N. Stoddard and M. Bertoni, "On the recombination centers of iron-gallium pairs in Ga-doped silicon," *J. Appl. Phys.,* vol. 122, *(8),* pp. 085703, 08/2017. DOI: 10.1063/1.5000358

[20] C. Vargas, Y. Zhu, G. Coletti, C. Chan, D. Payne, M. Jensen and Z. Hameiri, "Recombination parameters of lifetime-limiting carrier-induced defects in multicrystalline silicon for solar cells," *Appl. Phys. Lett.,* vol. 110, *(9),* pp. 092106, 03/2017. DOI: 10.1063/1.4977906

[21] J. Schön, A. Youssef, S. Park, L.E. Mundt, T. Niewelt, S. Mack, K. Nakajima, K. Morishita, R. Murai, M. Jensen, T. Buonassisi, M. Schubert, "Identification of lifetime limiting defects by temperature- and injection-dependent photoluminescence imaging," *J. Appl. Phys.,* vol. 120, *(10),* pp. 105703, 09/2016. DOI: 10.1063/1.4961465

[22] H. Bleichner, P. Jonsson, N. Keskitalo and E. Norlander, "Temperature and injection dependence of the Shockley–Read–Hall lifetime in electron irradiated n-type silicon," *J. Appl. Phys.,* vol. 79, *(12),* pp. 9142-9148, 06/1998. DOI: 10.1063/1.362585

[23] J. D. Murphy, K. Bothe, R. Krain, V. V. Voronkov and R. J. Falster, "Parameterisation of injection-dependent lifetime measurements in semiconductors in terms of Shockley-Read-Hall statistics: An application to oxide precipitates in silicon," *J. Appl. Phys.,* vol. 111, *(11),* pp. 113709, 06/2012. DOI: 10.1063/1.4725475

[24] S. Bernardini, T. U. Naerland, G. Colleti and M. Bertoni, "Defect Parameter Contour Mapping: A Powerful Tool for Lifetime Spectroscopy Data Analysis," *Submitted to Appl. Phys. Let.,* 2017.

[25] S. Rein, T. Rehrl, W. Warta and S. W. Glunz, "Lifetime spectroscopy for defect characterization: Systematic analysis of the possibilities and restrictions," *J. Appl. Phys.,* vol. 91, *(4),* pp. 2059-2070, 01/2002. DOI: 10.1063/1.1428095

[26] Y. Zhu, Q. T. L. Gia, M. K. Juhl, G. Coletti and Z. Hameiri, "Application of the Newton - Raphson Method to Lifetime Spectroscopy for Extraction of Defect Parameters," *IEEE Journal of Photovoltaics,* vol. 7, *(4),* pp. 1092-1097, 07/2017. DOI: 10.1109/JPHOTOV.2017.2695666

[27] K. Graff, *Metal Impurities in Silicon-Device Fabrication.* (2nd Edition ed.) Springer-Verlag Berlin Heidelberg, vol. 24, 1999. DOI: 10.1007/978-3-642-57121-3

[28] T. U. Naerland, "tnaerland/two_defect_DPCM_assessment: v1.0.0", 06/2017. DOI: 10.5281/zenodo.802992

[29] D. Macdonald and L. J. Geerligs, "Recombination activity of interstitial iron and other transition metal point defects in p- and n-type crystalline silicon," *Appl. Phys. Lett.,* vol. 85, *(18),* pp. 4061-4063, 09/2004. DOI: 10.1063/1.1812833

[30] S. Rein, *Lifetime Spectroscopy.* Springer-Verlag Berlin Heidelberg, vol. 85, 2005, DOI: 10.1007/3-540-27922-9

[31] A. L. Blum, J. S. Swirhun, R. A. Sinton, F. Yan, S. Herasimenka, T. Roth, K. Lauer, J. Haunschild, B. Lim, K. Bothe, Z. Hameiri, B. Seipel, R. Xiong, M. Dhamrin, J. D. Murphy, "Interlaboratory Study of Eddy-Current Measurement of Excess-Carrier Recombination Lifetime," *IEEE Journal of Photovoltaics,* vol. 4, *(1),* pp. 525-531, 10/2013. DOI: 10.1109/JPHOTOV.2013.2284375